Planar Ultra-Thin Small Beam-Switching Antenna

Long Zhang, Steven Gao, Senior Member, IEEE, Qi Luo, Member, IEEE, Paul R. Young, Senior Member, IEEE and Qingxia Li, Member, IEEE

Abstract—A novel planar ultra-thin electronically steerable parasitic array radiator (ESPAR) is presented in this paper. Through theoretical analysis of the electric fields of orthogonally crossed dipoles in phase quadrature, it is found that the crossed dipoles radiate linearly polarized (LP) wave with a rotational electric field in the azimuth plane. This characteristic is then utilized to design a planar crossed dipole ESPAR, termed as "CD-ESPAR". Furthermore, a simple but effective impedance matching method is also proposed and analyzed. To verify these concepts, a prototype with compact size and very low profile ($0.42\ \lambda_0 \times 0.42\ \lambda_0 \times 0.006\ \lambda_0$) resonating at 2.3GHz is designed, fabricated and measured. The measured results indicate that the proposed antenna achieves more than 17.8% impedance bandwidth and can produce four directional beams, covering the whole azimuth plane. Owing to its planar ultra-thin structure, compact size, electronically beam-switching ability, low power and low cost characteristics, it is promising for applications in wireless communications.

Index Terms—smart antenna, ESAPR, beam-switching, planar antenna, crossed dipoles.

I. Introduction

On the demand of high system capacity and improved quality of service (QoS), smart antennas have gained extensive interest during the last decade [1]. Typically, smart antenna systems can be categorized as either electronically switched-beam or adaptive-array systems [2]. Although the adaptive array has better performance than a switched-beam system, it comes at the expense of higher implementation cost and complexity constraints [3]. Therefore, for commercial applications such as personal wireless local network products, switched-beam systems are preferably deployed due to the low system complexity and low implementation cost.

Numerous beam-switching antennas and arrays for various applications were investigated. A classical method to produce switched beams is using the Butler matrix network. In [4], a 4×4 planar Butler matrix was implemented and integrated with four rectangular patches, which produces four different beams. However, the multi-port network of Butler matrix is rather bulky and complex. With the development of commercial semiconductor devices, it becomes increasingly popular to use low-cost switches such as the positive-intrinsic-negative (PIN) diodes in the development of low-cost feed networks for beam-switching antennas and arrays [5-7].

For commercial applications in wireless systems, it is necessary to develop innovative small smart antennas which have compact size and low cost. One potential technique is the electronically steerable parasitic array radiator (ESPAR), which consists of one driven element and several parasitic elements with reactive or resistive loads and only one radio frequency (RF) port [8-11]. By controlling the loads of parasitic elements, the beam direction of an ESPAR can be changed electronically. As ESPARs do not require any microwave phase shifters or a bulky, complicated feed network, it is promising for low-cost and low-power smart antenna applications.

ESPARs are initially designed to use dipoles as the driven and parasitic elements [10]. To reduce the height, monopoles were used [11]. However, the 0.25λ height of the monopoles is still large for some applications, especially for integration into mobile terminals. In [12], a homogeneous dielectric material is used to embed the antenna, which reduces the whole size of the antenna at the expense of efficiency degradation. Using folded monopoles or top-disk loaded monopoles can further reduce the height of ESPARs to about 0.1λ [9, 13, 14]. A low-profile multi-mode small antenna driven ESPAR with a height of 0.063λ is proposed in [15]. But in this design, a large ground plane is used which significantly increases the size of the antenna. Although these low-profile ESPARs work well, it is highly desired to design a planar ESPAR with antennas printed on a single substrate, which can facilitate the integration with RF front end and other components. However, there are few studies on such ESPAR designs up to now. In [16], patch antennas are utilized to obtain a planar ESPAR with steered conical beams in the elevation plane. A three-element patch array based ESPAR is proposed in [17], which achieves continuous scanning range of -15^o to 15^o in the elevation plane. Nevertheless, end-fire beams are preferable in some applications such as unmanned aerial vehicle (UAV) and wireless communications for azimuth signal coverage [18].

In this paper, orthogonally crossed dipoles in phase quadrature are employed to design a planar ultra-thin ESPAR, termed as "CD-ESPAR". This work is a further extension of our previous work in [19], where only some preliminary results using ideal RF switch models were given. In this paper, theoretical analysis of the operational principles, impedance matching method, and design methodology are presented with in-depth details. An antenna prototype with PIN diodes and the biasing circuit is designed, fabricated and full measurement

Manuscript received January 25, 2016.

L. Zhang, S. Gao, Q. Luo and P. R. Young are with the School of Engineering and Digital Arts, University of Kent, Canterbury CT2 7NT, UK. (emails: lz76@kent.ac.uk; s.gao@kent.ac.uk).

Q. Li is with the School of Electronic Information and Communications, Huazhong University of Science and Technology, Wuhan 430074, China.

results are provided. To show the advantages of the proposed design concept, a table that compares the present design with other reported ESPARs is given at the end of this paper. To the best knowledge of the authors, this is the first use of orthogonally crossed dipoles in phase quadrature to design a planar ultra-thin ESPAR with end-fire radiation patterns. Moreover, using the presented novel design method, the proposed "CD-ESPAR" has more compact size and lower profile compared with reported ESPARs.

The paper is organized as follows: Section II introduces the theoretical analysis of designing a beam-switching antenna using orthogonally crossed dipoles in phase quadrature; Section III presents the antenna configuration and impedance matching method; Section IV presents the simulation and measurement results and comparisons with other reported ESPARs. The conclusion is given in Section V.

II. Beam-Switching Antenna Using Orthogonally Crossed Dipoles in Phase Quadrature: Design and Theoretical Analysis

A. Radiated E-Field of Orthogonally Crossed Dipoles

As indicated in [20], the fields radiated by antennas of finite dimensions are spherical waves. To obtain the E-field of the crossed dipoles in far-field, spherical components E_r, E_φ and E_θ are adopted. As shown in Fig. 1, two dipoles with length of 2L are placed along X-axis and Y-axis respectively. Then, quadrature phase difference is given to these two dipoles. Here, the E-field of the crossed dipoles in azimuth plane (XOY plane) is deduced to explain the principles of the proposed method.

Based on the classical antenna theory [20], the E-field components radiated by the dipole placed along X-axis in the XOY plane can be written as

$$E_{r1} = 0,\ E_{\theta 1} = 0 \tag{1}$$

$$E_{\varphi 1} = j\eta \frac{I_1 e^{-jkr}}{2\pi r}\left[\frac{\cos(kL\cos\varphi)-\cos(kL)}{\sin\varphi}\right] \tag{2}$$

where η is the intrinsic impedance of the medium, which equals to 120π for free space; I_1 is the magnitude of electric current flowing along the dipole; k is the wave number.

Since a half-wavelength dipole is used, equation (2) can be rewritten as

$$E_{\varphi 1} = j\frac{60 I_1 e^{-jkr}}{r}\left[\frac{\cos\left(\frac{\pi}{2}\cos\varphi\right)}{\sin\varphi}\right] \tag{3}$$

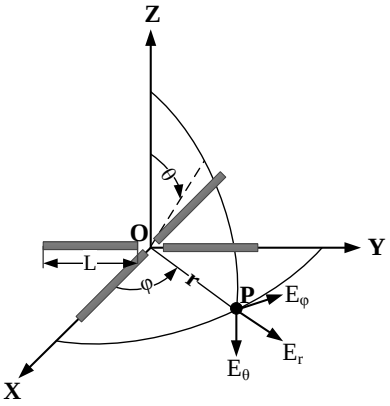

Fig. 1. Geometrical arrangement of crossed dipoles with quadrature phase difference and its associated electric-field components on a spherical surface.

Similar to the analysis in [21], the E-field components radiated by the second dipole placed along Y-axis in the XOY plane can be written as

$$E_{r2} = 0,\ E_{\theta 2} = 0 \tag{4}$$

$$E_{\varphi 2} = j\frac{60 I_2 e^{-jkr}}{r}\left[\frac{\cos\left(\frac{\pi}{2}\cos\left(\varphi-\frac{\pi}{2}\right)\right)}{\sin\left(\varphi-\frac{\pi}{2}\right)}\right] \tag{5}$$

where I_2 is the magnitude of electric current flowing along the second dipole.

The total E-field radiated by the crossed dipoles with quadrature phase difference in the XOY plane can be obtained by the vector superposition of the two separated E-field. Considering the phase centers of the two dipoles are both located at the original point O, the phase difference of the two separated E-field at the observation point P is thus only determined by the feeding phase difference of the two dipoles. Denoting the feeding phase difference by σ, the total E-field radiated by the orthogonally crossed dipoles in the XOY plane can be written as

$$\vec{E}(r,\theta,\varphi) = \overrightarrow{E_1}(r,\theta,\varphi) + \overrightarrow{E_2}(r,\theta,\varphi)\cdot e^{j\sigma} \tag{6}$$

Substituting (1)-(5) into (6) and (6) can be rewritten as

$$\vec{E}(r,\theta,\varphi) = \vec{\varphi} j\frac{60 I_1 e^{-jkr}}{r}\left[\frac{\cos\left(\frac{\pi}{2}\cos\varphi\right)}{\sin\varphi}\right] + \vec{\varphi} j\frac{60 I_2 e^{-jkr}}{r}\left[\frac{\cos\left(\frac{\pi}{2}\cos\left(\varphi-\frac{\pi}{2}\right)\right)}{\sin\left(\varphi-\frac{\pi}{2}\right)}\right] e^{j\sigma} \tag{7}$$

Assuming the magnitudes of the electric currents flowing on the two dipoles are the same, that is

$$I_1 = I_2 = I \tag{8}$$

Substituting (8) into (7) and using trigonometric identity, equation (7) reduces to

$$\vec{E}(r,\theta,\varphi) = \vec{\varphi} j\frac{60 I e^{-jkr}}{r}\left[\frac{\cos\left(\frac{\pi}{2}\cos\varphi\right)}{\sin\varphi} - \frac{\cos\left(\frac{\pi}{2}\sin\varphi\right)}{\cos\varphi}\cdot e^{j\sigma}\right] \tag{9}$$

Using Euler's formula, the normalized magnitude of $\vec{E}(r,\theta,\varphi)$ in XOY plane is

$$E = \sqrt{\left(\frac{\cos\left(\frac{\pi}{2}\cos\varphi\right)}{\sin\varphi} - \frac{\cos\sigma\cos\left(\frac{\pi}{2}\sin\varphi\right)}{\cos\varphi}\right)^2 + \frac{\sin^2\delta\cos^2\left(\frac{\pi}{2}\sin\varphi\right)}{\cos^2\varphi}} \tag{10}$$

Fig. 2 plots the normalized magnitude of the total E-field in XOY plane against azimuth angle φ under different values of σ.

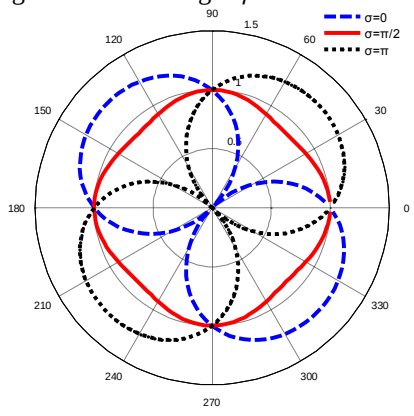

Fig. 2. The normalized magnitude of the total E-field in the azimuth plane.

From equations (9)-(10) and Fig. 2, it is concluded that:

1. The crossed dipoles with quadrature phase difference radiate linearly polarized (LP) fields at each specific

observation point in the azimuth plane (XOY plane). However, the orientation of the E-field rotates when the observation point changes along φ direction. This characteristic is the key point to produce switched beams through using orthogonally crossed dipoles in phase quadrature.

2. Compared with the normalized magnitude of the E-field as $\sigma = 0,\ \pi$, the magnitude of the E-field radiated by orthogonally crossed dipoles in phase quadrature ($\sigma = \pi/2$) is nonzero and relatively even at all azimuth angles. Therefore, it offers the possibility to produce directional beams towards any azimuth angles. On the contrary, a single dipole or crossed dipoles with 0^o or 180^o phase differences cannot be used to produce directional beams directing to any azimuth angles due to the existence of zero E-field in some areas. The detailed discussions on this are provided in the next sections.

B. Switched Beams Using Yagi-Uda Structure

As explained in section II A, the E-field of orthogonally crossed dipoles in phase quadrature in the azimuth plane is linearly polarized at each specific observation point in the far-field. For a LP E-field, it is conventional to use the Yagi-Uda array producing uni-directional radiation pattern [22]. By rotating the uni-direction pattern through some means, a switched beam antenna can be created. Besides, considering that the E-field radiated by orthogonally crossed dipoles in phase quadrature is nonzero in azimuth plane and always rotates along the azimuth angle φ, it is feasible to create an antenna with continuous switched beams or a directional beam pointing at any azimuth angle.

A schematic view of a switched beam antenna through rotating the reflector and the director to the orthogonally crossed dipoles is shown in Fig. 3. The rotation can be implemented by altering the function of parasitic elements between directors and reflector as described in [23]. By rotating the reflector and the director together with a rotating angle φ_r, the beam is expected to rotate as well.

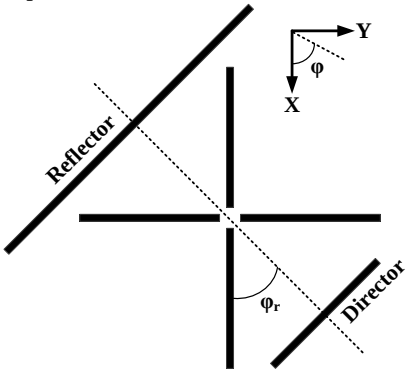

Fig. 3. Schematic view to create switched beams using orthogonally crossed dipoles driven Yagi-Uda array.

Fig. 4 gives the radiation patterns under different rotation angles φ_r. As shown, directional patterns are achieved in all cases. When φ_r changes, the main beam and the back lobe rotate as well. Since the magnitude of the rotating E-field radiated by orthogonally crossed dipoles in phase quadrature is non-zero at all azimuth angles as shown in Fig. 2, a continuous beam shift can be achieved when the reflector and director are rotated continuously. This characteristic gives obvious advantages compared with those beam-switching antennas utilizing a single dipole or crossed dipoles with in-phase or out-phase phase differences to form the Yagi-Uda antenna in terms of continuous beam-switching ability [23], as a single dipole based Yagi antennas only generate directional beams perpendicular to the dipole.

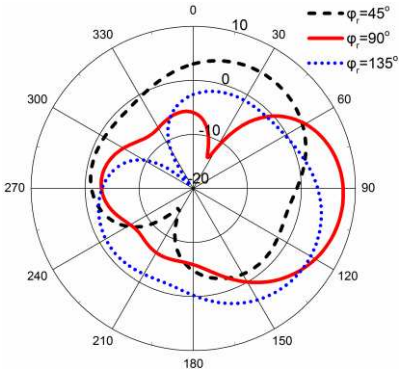

Fig. 4. Radiation patterns of a beam-switching Yagi antenna using orthogonally crossed dipoles in phase quadrature with different rotation angle φ_r.

C. Switched Beams Using ESPAR Structure

Although a theoretical method is proposed to produce switched beams using Yagi-Uda structure, it is complicated to realize as lots of switches such as PIN diodes are demanded to change the function of parasitic elements. An easier way to get switched beams is using the ESPAR structure.

A schematic view of crossed dipoles driven ESPAR ("CD-ESPAR") is shown in Fig. 5. As shown, orthogonally crossed dipoles in phase quadrature are enclosed by four parasitic dipoles. Each dipole is loaded by a varactor or a PIN diode. It is worth noticing that the driven crossed dipoles and the parasitic elements are in the same plane which is different to conventional ESPARs.

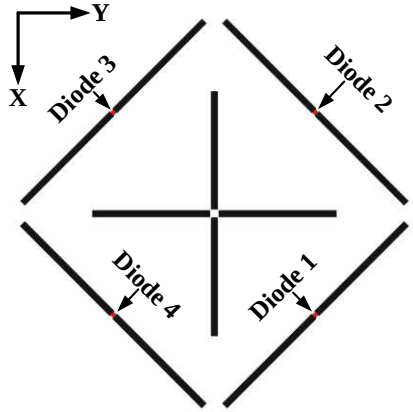

Fig. 5. Schematic view to create switched beams using orthogonally crossed dipoles in phase quadrature driven ESPAR (CD-ESPAR).

As analyzed in section Ⅱ A, the E-field radiated by the crossed dipoles is rotational and nonzero in the azimuth plane. This phenomenon indicates that the coupling between the crossed dipoles and the parasitic dipoles is non-zero once the parasitic elements are placed in the azimuth plane. The vertical

dipoles or monopoles used in conventional ESPARs are no longer needed, which results in a completely planar structure.

Although the proposed structure is totally different to those in [8, 9, 24], the operation principle to create switched beams is similar to the steering of the radiation pattern are all caused by controlling the coupling between the driven element and parasitic elements. Therefore, similar analysis method can be used to analyze the operation principles of the "CD-ESPAR".

The electric currents matrix $[I]$ on all parasitic elements and driven element can be calculated from the applied voltages matrix $[V]$ using the admittance matrix $[Y]$ or impedance matrix $[Z]$ [8, 9].

$$[I] = [Y] \times [V] = [Z]^{-1} \times [V] \tag{11}$$

where $[V] = [v_s \quad 0 \quad 0 \quad 0 \quad 0]$since only the driven element is excited and $[I] = [i_0 \quad i_1 \quad i_2 \quad i_3 \quad i_4]$.

The impedance matrix $[Z]$ can also be expressed as

$$[Z] = [Z_A] + [Z_L] \tag{12}$$

where $[Z_A]$ is a 5×5 impedance matrix denoting impedance of the driven element and parasitic elements including all mutual impedances and $[Z_L]$ is the load matrix for all elements

And $[Z_L]$ can be written as

$$[Z_L] = diag\left[0, R_1 + \frac{1}{j\omega c_1}, R_2 + \frac{1}{j\omega c_2}, R_3 + \frac{1}{j\omega c_3}, R_4 + \frac{1}{j\omega c_4}\right] \tag{13}$$

where R and C are the resistance and capacitance of the loads to each parasitic elements.

The far field directivity in the azimuth plane can be determined by the electric currents matrix $[I]$ through

$$\mathrm{D}(\varphi) = \frac{4\pi r^2}{\eta P_{input}} |E([I]^T \times \alpha(\varphi))|^2 \tag{14}$$

where r is the distance of the far field observation point to original point and P_{input} is the feeding power. $\alpha(\varphi)$ denotes the steering vector based on the array geometry

$$\alpha(\varphi) = \left[1 \;\; e^{j\frac{\pi}{2}\cos(\varphi)} \;\; e^{j\frac{\pi}{2}\cos\left(\varphi-\frac{\pi}{2}\right)} \;\; e^{j\frac{\pi}{2}\cos(\varphi-\pi)} \;\; e^{j\frac{\pi}{2}\cos\left(\varphi-\frac{3\pi}{2}\right)}\right]^T \tag{15}$$

From (11)-(15), it can be seen that changing the loads of the parasitic elements affects the electric currents on all elements. Once the electric currents matrix $[I]$ alters, the radiation pattern in the azimuth plane changes accordingly.

A schematic simulation has also been conducted to verify the proposed idea. The parasitic elements are loaded by PIN diodes. By turning on the four diodes sequentially, a beam-switching antenna with four directional patterns is realized, as shown in Fig. 6.

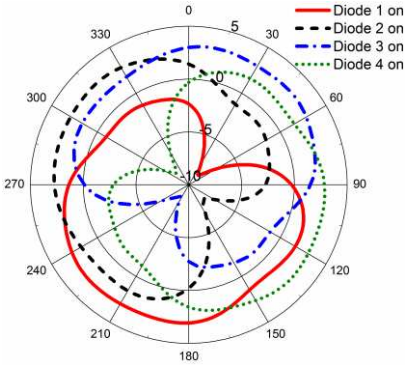

Fig. 6. Radiation patterns of an ESPAR using crossed dipoles as the driven element.

III. Antenna Configuration and Impedance Matching

In this section, the configuration of the proposed "CD-ESPAR" and the geometry dimensions are given at first. Then, the electric fields in the azimuth plane are given to verify the theoretical analysis in section Ⅱ. Finally, a simple but effective impedance matching method is proposed and analyzed.

A. Antenna Configuration

The antenna configuration along with the geometry dimensions are shown in Fig. 7. As shown in the figure, the antenna is etched on both sides of a 0.813mm thick Rogers RO4003C substrate with relative dielectric constant of 3.55 and dissipation factor of 0.0027. On the top layer, fan-shaped arm 1 and arm 2 are connected by a 3/4 ring-shaped phase delay line, which is then connected to the inner pin of the coaxial cable. The 3/4 ring-shaped line introduces 90 degrees phase differences between the crossed dipoles, which ensures the radiated E-field relatively even in the azimuth plane according to equation (10). Besides, a four-gap and four diodes loaded ring is placed outside the fan-shaped arms, which yields four parasitic elements. To control each PIN diode, two conductive lines are deployed perpendicularly to the ring. Within the direct current (DC) biasing lines for each diode, there are four inductors to choke the RF signal and one resistor to limit the current through the PIN diode.

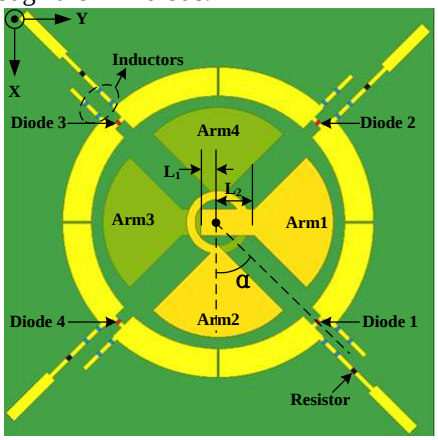

(a)

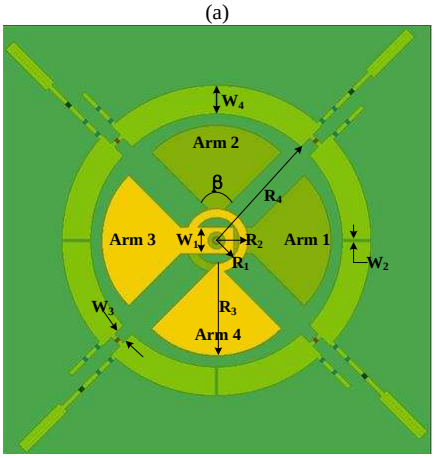

(b)

Fig. 7. Antenna configuration and dimensions: (a) top view, (b) bottom view.

On the bottom layer of the substrate, arm 3 and arm 4 are

connected to each other through the phase delay line and are placed symmetrically to arm 1 and arm 2, which constitutes the whole driven element. As the opposite fan-shaped arm pair constitutes a half-wavelength dipole, the electrical length of each fan-shaped arm should around $\lambda_g/4$ at the design frequency 2.3GHz. Both central angle β and radius R_3 determine the actual electrical length of the arm, which can be optimized by performing electromagnetic (EM) simulations. Since the driven element and the outer ring (parasitic elements) are placed closely and printed on one substrate, the whole structure features a compact size and very low profile.

The proposed antenna is designed to resonate at 2.3GHz and the detailed dimensions of the proposed antenna can be found in TABLE I.

TABLE I
ANTENNA PARAMETERS (MM)

R_1	R_2	R_3	R_4	W_1	W_2	W_3	W_4	L_1	L_2
4	5.5	16	22	4.5	0.42	2.13	5	3	6.25

Besides, the central angle β of each fan-shaped arm is 90°. The angle between the diode 1 and the center of arm 2 is denoted by α, which equals to 45°.

B. Radiated Fields of the Driven Element and the Proposed Antenna

As analyzed in section II, the radiated E-field of orthogonally crossed dipoles in phase quadrature is rotational in the azimuth plane. The detailed information about the radiated E-field of the driven element in XOY plane is indicated in Fig. 8.

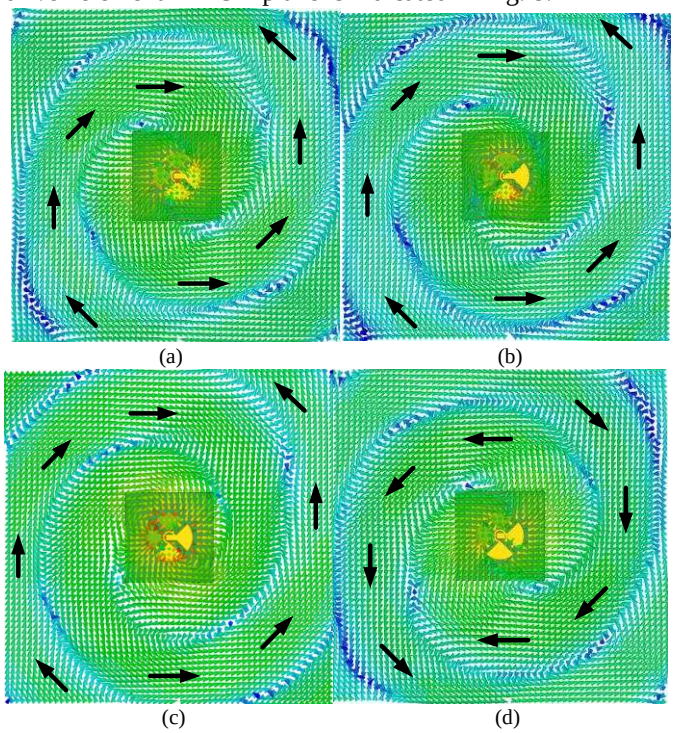

Fig. 8. The electric field distribution of the driven element in xoy plane at 2.3GHz: (a) 0°, (b) 45°, (c) 90°, (d) 180°.

Fig. 9 shows the E-field distribution of the proposed "CD-ESPAR" at 20mm height above the XOY plane when diode 1 is turned on. As can be seen, the magnitude of E-field degrades in the vicinity of diode 1 and gets strengthened in the opposite direction, which results in a directional radiation pattern in the azimuth plane. The variation of the E-fields' magnitude is caused by the coupling between the driven element and the parasitic ring, which is analyzed in section Ⅱ C. By turning on the diodes sequentially, a beam-switching antenna can be achieved.

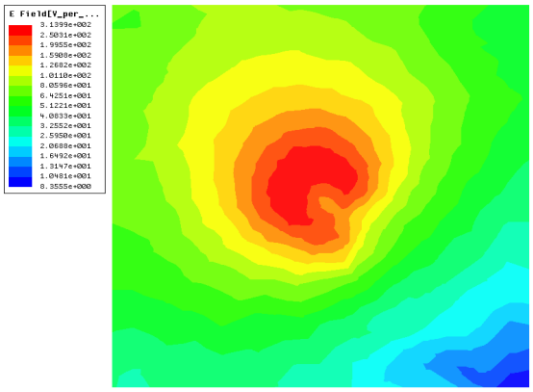

Fig. 9. The electric field distribution of the proposed antenna at 2.3GHz.

C. Impedance Matching

ESPARs are tightly coupled structures and the input impedance of the driven element is strongly affected by the capacitive loading of the parasitic elements [9]. Normally, eliminating the capacitive loading can achieve good impedance matching. Unlike other studies, in this design, more capacitance is introduced to the driven element of the "CD-ESPAR" and a good impedance matching is also observed.

The proposed impedance matching method is effective and easy to implement. To explain the method, a magnified picture of the partly overlapped rectangular patch used in the driven element is given by Fig. 10. As shown in the picture, the pair of rectangular patches is printed on both sides of the substrate with an overlapped area of $W_1 \times L_1$. This overlapped structure of two patches results in a pair of parallel-plate capacitors, i.e. capacitor C_1 and C_2 shown in Fig. 10. It is found that these two capacitors can effectively enhance the impedance characteristics of the proposed antenna and thus broaden the antenna's bandwidth.

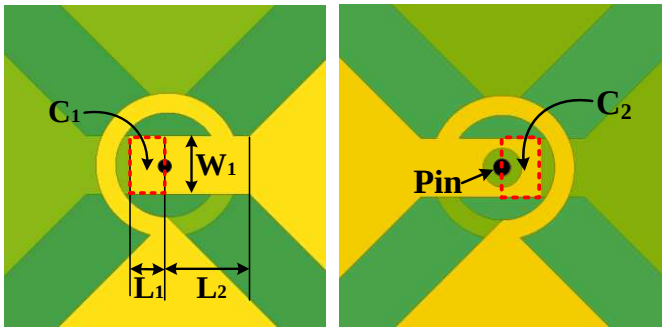

Fig. 10. Configuration of overlapped rectangular patch: (a) top view, (b) bottom view.

To analyze the proposed impedance matching mechanism, qualitatively, the equivalent circuit model of the antenna is provided in Fig. 11. The symbol Y_A denotes the antenna admittance without the overlapped rectangular patches while

C_1 and C_2 denote the parallel-plate capacitors and Y_{in} represents the total input admittance of the proposed antenna.

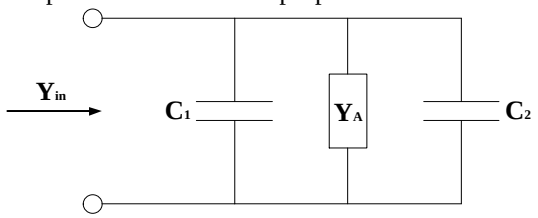

Fig. 11. Equivalent circuit model of the proposed antenna.

The capacitance of parallel-plate capacitors C_1 and C_2 can be calculated when the electric charge density on the plates is uniform and the fringing fields at the edges can be neglected. From Fig. 11, the input admittance Y_{in} of the proposed antenna can be denoted by:

$$Y_{in} = Y_A + j\omega(C_1 + C_2) \approx Y_A + 2j\omega\frac{\varepsilon_r\varepsilon_0 W_1 L_1}{\mathrm{h}} \qquad (16)$$

The approximation derives from the small slot on bottom rectangular patch which decreases the overlapped area of the two parallel-plate capacitors.

It is shown in equation (16) that the antenna input admittance Y_{in} is determined by the rectangular patch width W_1 and length L_1. Therefore, the impedance characteristic of the antenna can be tuned by these two parameters to achieve a good impedance matching.

In order to demonstrate, intuitively, the effect of changing parameters W_1 and L_1, the simulated input impedances under different W_1 and L_1 are studied while keeping the other antenna geometry parameters fixed.

The simulated input impedance of the proposed antenna for various values of L_1 is shown in Fig. 12. As can be seen from Fig. 12, the input impedance without the overlapped patch (case L_1 = 0 mm) is mainly inductively and the majority of the impedance loci falls outside the voltage standing wave ratio (VSWR) = 2 circle, indicating that the bandwidth at this state is very narrow. The inductive input impedance may stem from the inner pin of the coaxial line, which goes through the substrate and introduces some inductance. The ring-shaped phase delayed line may bring some inductance as well. By increasing L_1, the impedance locus begins to move along the admittance circle due to the increasing capacitance of C_1 and C_2. This phenomenon can be well explained by equation (16) as well.

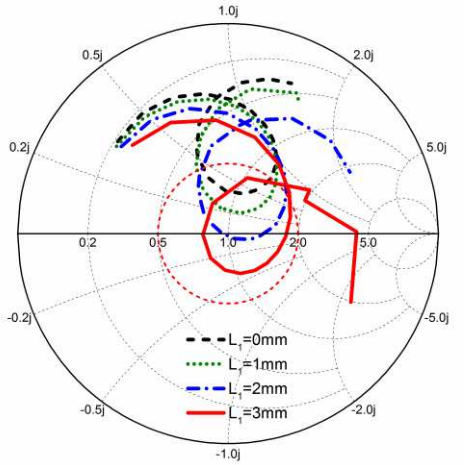

Fig. 12. Simulated input impedance of the proposed antenna with different L_1.

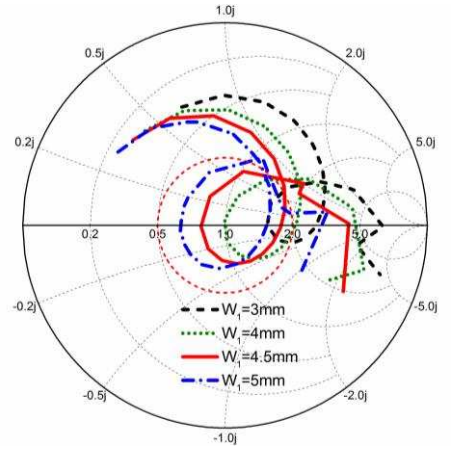

Fig. 13. Simulated input impedance of the proposed antenna with different W_1.

Fig. 13 depicts the input impedance loci under different patch widths, W_1, when patch length L_1 is 3 mm. Similar to the phenomenon observed in Fig. 12, the impedance loci will move along the admittance circle when W_1 becomes larger. This impedance matching procedure is similar to the method using lumped LC elements to tune the impedance bandwidth. However, the proposed method is more advantageous in terms of antenna efficiency and complexity due to the absence of a lossy π-type or M-type LC circuit.

D. Parametric Study of R_4

The distance between the diodes and the phase center of the dipoles is represented by the geometry parameters R_4. The variation of R_4 affects the mutual coupling between the crossed dipoles and the outer parasitic ring, which influences the far-field radiation as explained in section II C. To give a better understanding of how R_4 affects the performance of the antenna, Fig. 14 gives the simulated directivity and the front to back ratio (FBR) of the present antenna under different values of R_4. As can be seen from Fig.14, the directivity increases when R_4 increases. However, the FBR decreases in this case. To obtain large FBR and moderate antenna gain, the parameter R_4 is chosen to be 22mm.

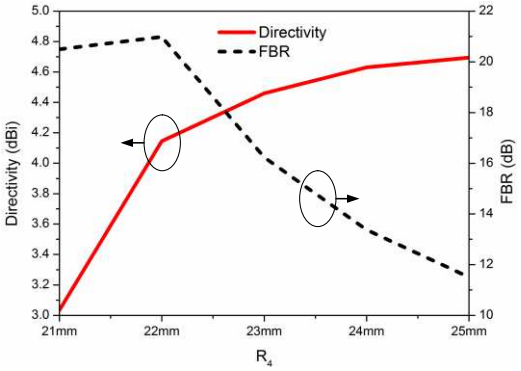

Fig. 14. The simulated directivity and FBR under different R_4 at 2.3GHz

IV. Results and Discussions

A. Reflection Coefficient

A prototype is fabricated and measured to verify the performance of the proposed antenna. As shown in Fig. 15, the

four diodes are controlled by four button batteries which are positioned at the four corners of the substrate. Two Skyworks SMP1345-079LF PIN diodes with small capacitance (0.15pf) and series resistance (1Ω) are used in the prototype. To choke the RF current flowing into the bias line, two 33nH inductors are built into each line. Besides, a 47Ω lumped resistor is embedded into each bias line and a 1.5V button cell battery is used to bias the pin diode, which gives around 32mA DC current.

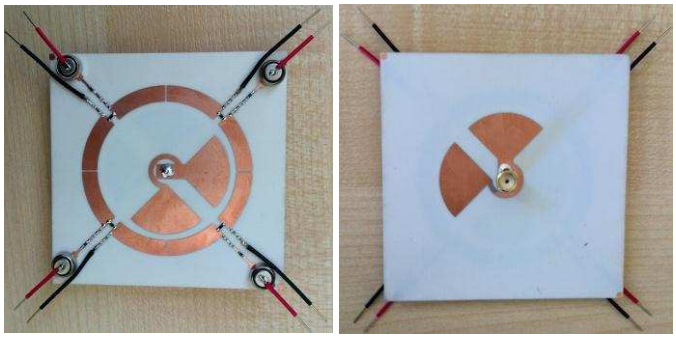

(a) (b)

Fig. 15. The prototype of the proposed antenna: (a) top view, (b) bottom view.

The simulated and measured reflection coefficient is shown in Fig. 16 and Fig. 17, respectively. The measured results indicate that the proposed antenna operates from 2.24GHz to 2.68GHz when diode 2 or 4 is turned on and from 2.25GHz to 2.98GHz when diode 1 or 3 is turned on. Notice that there are obvious differences between the results obtained from the case diode 1 or 3 is on and the case diode 2 or 4 is on. These differences are caused by the asymmetric structure of the proposed antenna. Although the antenna is composed of four symmetric arms (driven element) and a rotational symmetric parasitic ring, the dual-layer structure of the driven element results in different coupling magnitude. More specifically, arm 1, 2 are on the same layer and arm 1, 4 are on the different layer, therefore the coupling between arm 1, 2 and the parasitic ring is different to the coupling between arm 1, 4 and the parasitic ring.

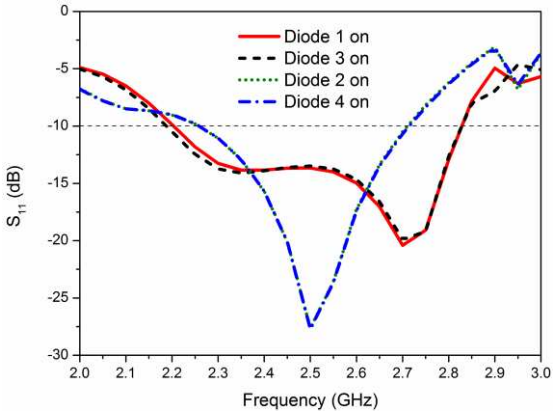

Fig. 16. Simulated reflection coefficient under four states.

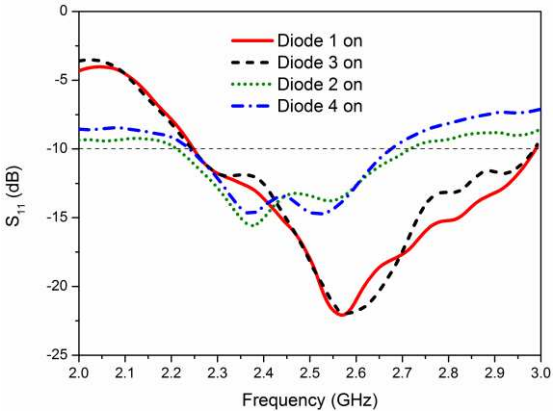

Fig. 17. Measured reflection coefficient under four states.

B. Radiation Pattern

The simulated and measured radiation patterns in the XOY plane (azimuth plane) at 2.3GHz are shown in Fig. 18. As can be observed in Fig. 18, four directional beams can be produced

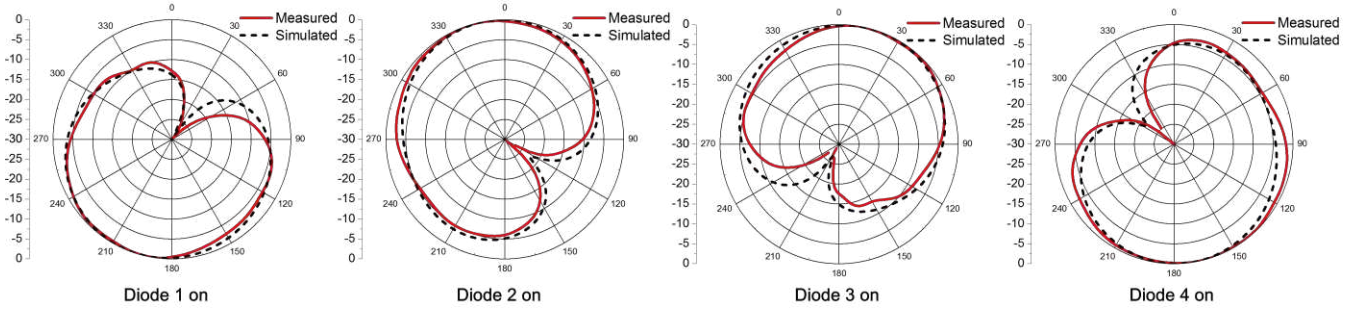

Fig. 18. Simulated and measured radiation patterns in the azimuth plane at 2.3GHz.

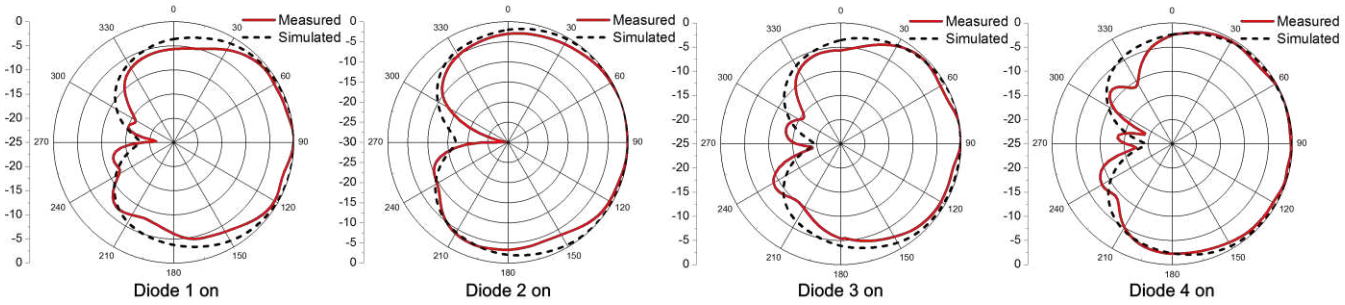

Fig. 19. Simulated and measured radiation patterns in the elevation plane at 2.3GHz.

in the azimuth plane. The measured radiation patterns indicate that the antenna has a 3dB beam width of about 120 degrees which makes the proposed antenna able to fulfill the whole azimuth coverage requirement. Besides, the measured antenna gain is about 3.5dBi under all states while the simulated realized gain is around 3.85dBi. Moreover, the measured FBR is larger than 20dB. The high FBR enables the antenna suitable for applications such as interference rejection in wireless communications.

Fig. 19 shows the measured and simulated radiation patterns in the elevation plane. Good agreement between the simulation and measurement results can be observed. Moreover, end-fire radiation can also be observed through Fig. 19.

The radiation patterns at different frequency points are shown in Fig. 20. As shown, the radiation patterns vary slightly when the frequency changes.

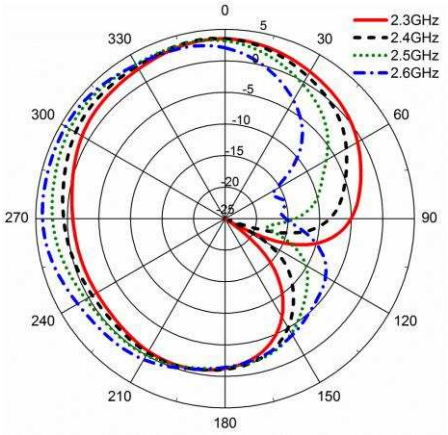

Fig. 20. Radiation patterns at different frequency points when diode 2 is turned on.

As indicated in section III A, the phase delay between the crossed dipoles is introduced by the ring-shaped phase delay line. When the frequency shifts from 2.3GHz to 2.6GHz, the phase difference σ changes from $\frac{\pi}{2}$ to $\frac{\pi}{2}\times\frac{2.6}{2.3}$. From equation (10), a variation of σ results in the variation of the magnitude of the E-field in XOY plane. Once the radiated E-field by the crossed dipoles changes, the mutual coupling between the driven crossed dipoles and the parasitic ring changes as well. According to equations (11) and (12), the currents matrix [I] varies as the impedance matrix $[Z_A]$ which relates to the mutual coupling changes. Subsequently, the far-field radiation of the "CD-ESPAR" also alters according to equation (14).

C. Comparison with Other Reported ESPARs

To illustrate the advantages of the proposed "CD-ESPAR", a comparison with other reported ESPARs in terms of antenna size, antenna height, antenna gain, antenna bandwidth (BW) and beam-switching ability is given in Table II. The ground planes used in conventional ESPARs such as in [8, 9, 13] are not taken into account, which means that the actual overall size and height of the antenna are larger than what are given in the table . From the table, it is clear that the proposed "CD-ESPAR" possesses more compact size, larger bandwidth and lower profile while maintaining beam-switching capability and full azimuth plane coverage.

Table II
COMPARISON OF ESPARS

Ref. No.	Size	Height	Main Beam Direction	Azimuth Coverage	Gain	BW
[8]	0.5λ ×0.5λ	0.25λ	Azimuth Plane	Yes	-	1.2%
[9]	0.4**λ** ×0.4**λ**	0.1**λ**	Azimuth Plane	Yes	4dBi	10.3%
[13]	1.44 **λ** ×1.44**λ**	0.2**λ**	Azimuth Plane	Yes	10 dBi	6.3%
[16]	0.96 **λ** ×0.96**λ**	0.025**λ**	Elevation Plane	No	5.78 dBi	0.7%
[17]	0.8**λ** ×0.3**λ**	0.01**λ**	Elevation Plane	No	6.5 dBi	~1.5%
This Work	0.42**λ** ×0.42**λ**	0.006**λ**	Azimuth Plane	Yes	3.5 dBi	17.9%

V. CONCLUSION

A planar ultra-thin small "CD-ESPAR" is proposed in this paper. Unlike conventional ESPARs, the proposed antenna uses orthogonally crossed dipoles in phase quadrature to create end-fire switched beams. This novel method makes designing completely planar ESPARs with very low profile feasible. Moreover, fan-shaped crossed dipoles and ring-shaped parasitic elements are employed, which further reduces the antenna size. The proposed antenna produces four switchable radiation patterns with more than 20dB FBR. Compared with other reported ESPARs, the proposed antenna has more compact size and much lower antenna height while maintaining electronically beam-switching capability, which makes the antenna suitable for applications in wireless communications.

REFERENCES

[1] S. Bellofiore, C. A. Balanis, J. Foutz, and A. S. Spa, "Smart-antenna systems for mobile communication networks. Part 1. Overview and antenna design," IEEE Antennas Propag. Mag., vol. 44, pp. 145-154, 2002.

[2] M. Chryssomallis, "Smart antennas," IEEE Antennas Propag. Mag., vol. 42, pp. 129-136, 2000.

[3] Z. Zhang, M. F. Iskander, Z. Yun, and A. Høst-Madsen, "Hybrid smart antenna system using directional elements-performance analysis in flat Rayleigh fading," IEEE Trans. Antennas Propag., vol. 51, pp. 2926-2935, 2003.

[4] C.-H. Tseng, C.-J. Chen, and T.-H. Chu, "A low-cost 60-GHz switched-beam patch antenna array with Butler matrix network," IEEE Antennas Wireless Propag. Lett., vol. 7, pp. 432-435, 2008.

[5] W. C. Zheng, L. Zhang, Q. X. Li, and Y. Leng, "Dual-band dual-polarized compact bowtie antenna array for anti-interference MIMO WLAN," IEEE Trans. Antennas Propag., vol. 62, pp. 237-246, 2014.

[6] A.-D. Capobianco, F. M. Pigozzo, A. Assalini, M. Midrio, S. Boscolo, and F. Sacchetto, "A compact MIMO array of planar end-fire antennas for WLAN applications," IEEE Trans. Antennas Propag., vol. 59, pp. 3462-3465, 2011.

[7] M. Maqsood, S. Gao, T. W. Brown, M. Unwin, R. De Vos Van Steenwijk, J. Xu, et al., "Low-cost dual-band circularly polarized switched-beam array for global navigation satellite system," IEEE Trans. Antennas Propag., vol. 62, pp. 1975-1982, 2014.

[8] C. Sun, A. Hirata, T. Ohira, and N. C. Karmakar, "Fast beamforming of electronically steerable parasitic array radiator antennas: theory and experiment," IEEE Trans. Antennas Propag., vol. 52, pp. 1819-1832, 2004.

[9] H.-T. Liu, S. Gao, and T.-H. Loh, "Electrically small and low cost smart antenna for wireless communication," IEEE Trans. Antennas Propag., vol. 60, pp. 1540-1549, 2012.

[10] R. F. Harrington, "Reactively controlled directive arrays," IEEE Trans. Antennas Propag., vol. 26, pp. 390-395, 1978.
[11] R. Schlub, J. Lu, and T. Ohira, "Seven-element ground skirt monopole ESPAR antenna design from a genetic algorithm and the finite element method," IEEE Trans. Antennas Propag., vol. 51, pp. 3033-3039, 2003.
[12] J. Lu, D. Ireland, and R. Schlub, "Dielectric Embedded ESPAR (DE-ESPAR) antenna array for wireless communications," IEEE Trans. Antennas Propag., vol. 53, pp. 2437-2443, 2005.
[13] H. Liu, S. Gao, and T.-H. Loh, "Small director array for low-profile smart antennas achieving higher gain," IEEE Trans. Antennas Propag., vol. 61, pp. 162-168, 2013.
[14] H. Liu, S. Gao, and T. H. Loh, "Compact dual-band antenna with electronic beam-steering and beamforming capability," IEEE Antennas Wireless Propag. Lett., vol. 10, pp. 1349-1352, 2011.
[15] L. Akhoondzadeh-Asl, J.-J. Laurin, and A. Mirkamali, "A Novel Low-Profile Monopole Antenna With Beam Switching Capabilities," IEEE Trans. Antennas Propag., vol. 62, pp. 1212-1220, 2014.
[16] W. Chen, J. Sun, X. Wang, Z. Feng, F. Chen, Y. Furuya, et al., "A novel planar switched parasitic array antenna with steered conical pattern," IEEE Trans. Antennas Propag., vol. 55, pp. 1883-1887, 2007.
[17] J. J. Luther, S. Ebadi, and X. Gong, "A microstrip patch electronically steerable parasitic array radiator (ESPAR) antenna with reactance-tuned coupling and maintained resonance," IEEE Trans. Antennas Propag., vol. 60, pp. 1803-1813, 2012.
[18] Z. Chen and Z. Shen, "Wideband Flush-Mounted Surface Wave Antenna of Very Low Profile," IEEE Trans. Antennas Propag., vol. 63, pp. 2430 - 2438, 2015.
[19] L. Zhang, S. Gao, Q. Luo, and Y. Geng, "Low-profile compact-size electronically beam-switching antenna for wireless communications," in Proc. 9th Eur. Conf. Antennas Propag. (EuCAP), 2015.
[20] C. A. Balanis, Antenna theory: analysis and design vol. 1: John Wiley & Sons, 2005.
[21] Y. Luo, Q.-X. Chu, and L. Zhu, "A Low-Profile Wide-Beamwidth Circularly-Polarized Antenna via Two Pairs of Parallel Dipoles in a Square Contour," IEEE Trans. Antennas Propag., vol. 63, pp. 931-936, 2015.
[22] N. Kaneda, W. Deal, Y. Qian, R. Waterhouse, and T. Itoh, "A broadband planar quasi-Yagi antenna," IEEE Trans. Antennas Propag., vol. 50, pp. 1158-1160, 2002.
[23] C. Kittiyanpunya and M. Krairiksh, "A four-beam pattern reconfigurable Yagi-Uda antenna," IEEE Trans. Antennas Propag., vol. 61, pp. 6210-6214, 2013.
[24] S. Sugiura and H. Iizuka, "Reactively steered ring antenna array for automotive application," IEEE Trans. Antennas Propag., vol. 55, pp. 1902-1908, 2007.

Long Zhang received the B.S. and M.S. degrees in electrical engineering from Huazhong University of Science and Technology (HUST), Wuhan, China, in 2009 and 2012, respectively. He is currently pursuing the Ph.D. degree at the University of Kent, Canterbury, U.K.

He was an Antenna Engineer with Huawei in 2012 and then a Graduate Research Assistant with the Multi-Spectral Information Processing Laboratory, HUST, in 2013. His research interests include circularly polarized antennas and arrays, smart antennas, reconfigurable antennas, mobile terminal antennas, and reflectarray.

Steven Gao (M'01–SM'16) received the Ph.D. degree in microwave engineering from Shanghai University, Shanghai, China, in 1999.

He is a Professor and Chair in RF and microwave engineering with the University of Kent, Canterbury, U.K. He co-authored two books including Space Antenna Handbook (Wiley, 2012) and Circularly Polarized Antennas (IEEE-Wiley, 2014), published more than 250 papers, and holds several patents in smart antennas and RF. His research interests include smart antennas, phased arrays, satellite antennas, RF/microwave/mm-wave/THz circuits, satellite communications, UWB radars, synthetic-aperture radars, and mobile communications.

Dr. Gao is a Distinguished Lecturer of the IEEE AP Society and serves as an Associate Editor for a number of international journals including the IEEE TRANSACTIONS ON ANTENNAS AND PROPAGATION and Radio Science. He has given invited talks or plenary talks at some international conferences and was a General Chair of LAPC 2013, U.K.

Qi Luo (S'08–M'12) received the M.Sc degree in data communications from the University of Sheffield, Sheffield, U.K., in 2006; and the Ph.D. degree in electrical engineering from the University of Porto, Porto, Portugal, in 2012.

From 2012 to 2013, he was a Research Fellow with the Surrey Space Centre, Guildford, U.K. Currently, he is a Research Associate with the School of Engineering and Digital Arts, University of Kent, Canterbury, U.K. His research interests include smart antennas, circularly polarized antennas, reflectarray, multiband microstrip antennas, and electrically small antenna design.

Paul R. Young (M'00–SM'05) received the B.Eng. and Ph.D. degrees in electronic engineering from the University of Kent, Canterbury, Kent, U.K., in 1994 and 1998, respectively.

From 1997 to 1999, he was a Research Scientist with the National Physical Laboratory, Middlesex, U.K., where he developed standards for RF and microwave impedance measurement. He then spent a year as a Research Fellow with the University of Surrey before becoming a Lecturer with the University of Kent in 2001. He has authored or coauthored over 40 papers in journals and conference proceedings. His research interests include guided-wave structures, electromagnetic bandgaps, and microwave measurement techniques.

Qingxia Li (M'08) received the B.S., M.S., and Ph.D. degrees in electrical engineering from Huazhong University of Science and Technology (HUST), Wuhan, China, in 1987, 1990, and 1999, respectively.

He is currently a Professor in Science and Technology on Multi-Spectral Information Processing Laboratory, School of Electronic Information and Communications, HUST. His current research interests include microwave remote sensing and deep space exploration, electromagnetic theory and application, antenna array and signal processing.